Journal of Electronic Materials (2022) 51:1933–1939
https://doi.org/10.1007/s11664-022-09551-5

TOPICAL COLLECTION: SYNTHESIS AND ADVANCED CHARACTERIZATION OF MAGNETIC OXIDES

Spinel Ferrites ($CoFe_2O_4$): Synthesis, Magnetic Properties, and Electromagnetic Generator for Vibration Energy Harvesting

Yumi Oh[1] · Manisha Sahu[1] · Sugato Hajra[1] · Aneeta Manjari Padhan[1] · Swati Panda[1] · Hoe Joon Kim[1,2]

Received: 10 December 2021 / Accepted: 22 February 2022 / Published online: 15 March 2022

Abstract
Cobalt ferrite bearing the chemical formula of $CoFe_2O_4$ was synthesized by a high-temperature solid-state reaction. The Rietveld refinement of the experimental XRD data shows that the synthesized material crystallizes in a cubic symmetry with a lattice parameter a = b = c = 8.391 Å. The magnetic property of $CoFe_2O_4$ reveals the maximum magnetization value of 84.17 emu/g, confirming a strong ferrimagnetic nature. Further, we have built an electromagnetic energy generator (EMG) device based on the $CoFe_2O_4$ magnetic material, copper coil, and three-dimensional (3D) printed tube-like structure. The electrical output response of the device was collected by shaking it by hand and an electric shaker. A voltage of 1.95 V and current of 4.7 mA was generated from the device while delivering a power output as high as 0.86 mW at a load resistance of 10^3 Ω. The electrical output remained constant over long-term device operation, confirming that the fabricated device is capable of generating a stable output for a longer duration. Powering of light-emitting diodes (LEDs) and charging of capacitors were performed by utilizing the fabricated EMG. Further, the self-powered recognition of different speeds when the device was placed upon an electric shaker confirms that it can be utilized in many real-time applications.

Keywords Spinel ferrites · magnetic · electromagnetic · energy harvesting

Introduction

The spinel (having general formula AB_2O_4) structured ferrites, a significant class of magnetic materials, have attracted widespread scientific recognition in recent decades due to their potential applications in the fields of actuators, sensors, solar cells, high-density magnetic recording, data storage, and spintronics.[1–3] Among these, cobalt ferrite ($CoFe_2O_4$) has been widely studied due to its large magnetostriction, high coercivity and saturation magnetization, high cubic magneto-crystalline anisotropy, and excellent chemical stability.[4–6] $CoFe_2O_4$ can have a normal or an inverse spinel structure depending upon the position of its cations.[7,8] The O^{2-} ions form a face-centered cubic lattice, and the Co^{2+} and Fe^{3+} ions occupy either tetrahedral or octahedral interstitial sites. Here, the cationic distribution is expressed as $(Co_{1-\delta}Fe_{\delta})_{Td}$ $[Co_{\delta}Fe_{2-\delta}]_{Oh}$, and the cations within the round and square bracket occupy the tetrahedral and octahedral sites, respectively. The symbol (δ) denotes the degree of inversion parameter that depends on sample preparation conditions. The value of δ remains zero for the normal spinels ($\delta = 0$), where the Co^{2+} and Fe^{3+} ions occupy the tetrahedral (T_d) and octahedral (O_h) sites, respectively. On the other hand, in the inverse spinel structure of $CoFe_2O_4$ ($\delta = 1$), Co^{2+} ions and half of the Fe^{3+} ions occupy the octahedral sites, while the remaining half of Fe^{3+} ions situate in the tetrahedral sites.[9] Therefore, the overall magnetic property is contributed from the two antiparallel sublattices coupled by the strong super-exchange interactions via the O^{2-} ions and depict a ferrimagnetic behavior.[10]

Energy-harvesting technologies have drawn much attention in modern days in the fields of environmental

Yumi Oh, Manisha Sahu, and Sugato Hajra have contributed equally to this work.

✉ Hoe Joon Kim
joonkim@dgist.ac.kr

[1] Department of Robotics Engineering, Daegu Gyeongbuk Institute of Science and Technology (DGIST), Daegu 42988, Republic of Korea

[2] Robotics Research Center, Daegu Gyeongbuk Institute of Science and Technology (DGIST), Daegu 42988, Republic of Korea

monitoring and the internet of things (IoT) to build a battery-free sensor system.[11] Various nano- or micro-generators based on piezoelectric, triboelectric, and electromagnetic effects are becoming popular to design and realize many self-powered applications.[12–15] Nature provides a wide variety of vibrations and impacts in the form of mechanical energy. Effective conversion of these waste energies could produce useful electrical energy. The low frequency and irregular nature of machine vibrations or human motions are hard to convert into electrical energy using a resonant generator, and it is necessary to find an alternative generator that operates in a non-sinusoidal random vibration. Electromagnetic generators (EMGs) provide numerous advantages such as several possible architectures for device fabrication, higher current output, low impedance, and operation in all modes of a low-, medium-, or high-frequency vibration.[16] The piezoelectric nanogenerators are not suited to harvest energy from very low-frequency sources, as efficient energy conversion is possible at higher frequency ranges (60–100 Hz or more).[17] Triboelectric nanogenerators and EMGs can be beneficial for low-frequency energy harvesting. $CoFe_2O_4$-based nanogenerators have been rarely investigated in the past, so it is an interesting approach to shed light upon applying the synthesized materials for energy harvesting. However, reports show $CoFe_2O_4$ usage requires a single compound or composite form for use in gas sensors, supercapacitors, and magnetic sensors.[18–20] Table S1 shows the comparison of the EMGs and their electrical responses such as voltage, current, and power.

In this work, a spinel ferrite (cobalt ferrite) was synthesized using a solid-state reaction, and various material characterizations were conducted to correlate the material properties along with an energy-harvesting device fabrication. A facile three-dimensional (3D) printing technology was used to develop the housing for the electromagnetic generator, while copper coil wire was wrapped around the housing. Finally, the magnetic material (cobalt ferrite) was placed inside the housing to convert the mechanical shaking vibration into electrical energy. Various demonstrations of the electrical response of the device were carried out to confirm the stability of the device, its powering of LEDs, and charging of capacitors. The EMG device was attached to the vibration shaker, and the electrical response was recorded at different speeds of shaking, elucidating its usage in understanding machine smooth functioning or faults.

Material Synthesis and Characterization

The solid-state reaction method was employed to synthesize bulk $CoFe_2O_4$ power. The cobalt oxide and iron (III) oxide having high purity >99 % were purchased from Alfa Aesar, South Korea, and utilized for the chemical reaction without further purification. The oxide powders were taken carefully in estimated stoichiometry using a digital balance and transferred into an agate mortar and pestle. The powders were mixed in the presence of methanol for 2 h until a homogenous mixture was obtained. Further, this mixture was poured into a crucible placed inside a high-temperature furnace for calcination at 1200°C for 4 h. The synthesized powder was confirmed by x-ray diffraction (XRD) to gain insight into its phase formation. After that, the powder and polyvinyl alcohol (PVA) were mixed properly, which acted as a binder, and then a hydraulic press was utilized to make a cylindrical type of pellets having a dimension of 13 mm and thickness of 1.5 mm. These green pellets were sintered at a higher temperature of 1250°C for 4 h and directly utilized as a magnetic material to design the electromagnetic generator.

XRD analysis was carried out to understand the structural formation and crystallographic parameters using a powder x-ray diffractometer (M/S Malvern Panalytical, UK) having Cu-K_α radiation and step size of 3°/min. The surface morphology was captured by using a scanning electron microscope (M/S Hitachi S-4900, Tokyo) at an accelerating voltage of 15 kV. The pellet was coated with highly conductive silver paint in a metal–dielectric–metal arrangement, and the dielectric properties were evaluated with the help of an impedance analyzer (M/S Hioki IM3470, Tokyo). The molecular structure was determined with the help of the .CIF file and the crystallographic parameters achieved from XRD analysis. The elemental mapping and energy-dispersive x-ray spectroscopy (EDS) spectra were obtained from the scanning electron microscope attached to the Bruker EDS system. The magnetic property of the synthesized particles was assessed at room temperature using a vibrating sample magnetometer (VSM, Lakeshore 7407, USA) having a field range of ± 17 kOe. The voltage and current of the electromagnetic generator were measured using an electrometer equipped with the Labview program. A NdFeB magnet was used with the $CoFe_2O_4$ pellets to polarize the magnetic pellet.

Results and Discussions

Figure 1a shows the step-by-step process to synthesize the $CoFe_2O_4$ particles. The starting ingredients, such as oxides, were taken in a proper ratio and mixed in an agate mortar pestle until a homogenous mixture was achieved. Then, the mixture was transferred into a crucible and put inside a furnace (1200°C for 4 h) for calcination. The lump was formed, and then it was again ground into fine powders, which were pressed into disk pellets and utilized for characterization. Figure 1b shows the layer-by-layer fabrication step to build an EMG device. The tube-shaped housing was 3D-printed using an Ultimaker 3S 3D printer

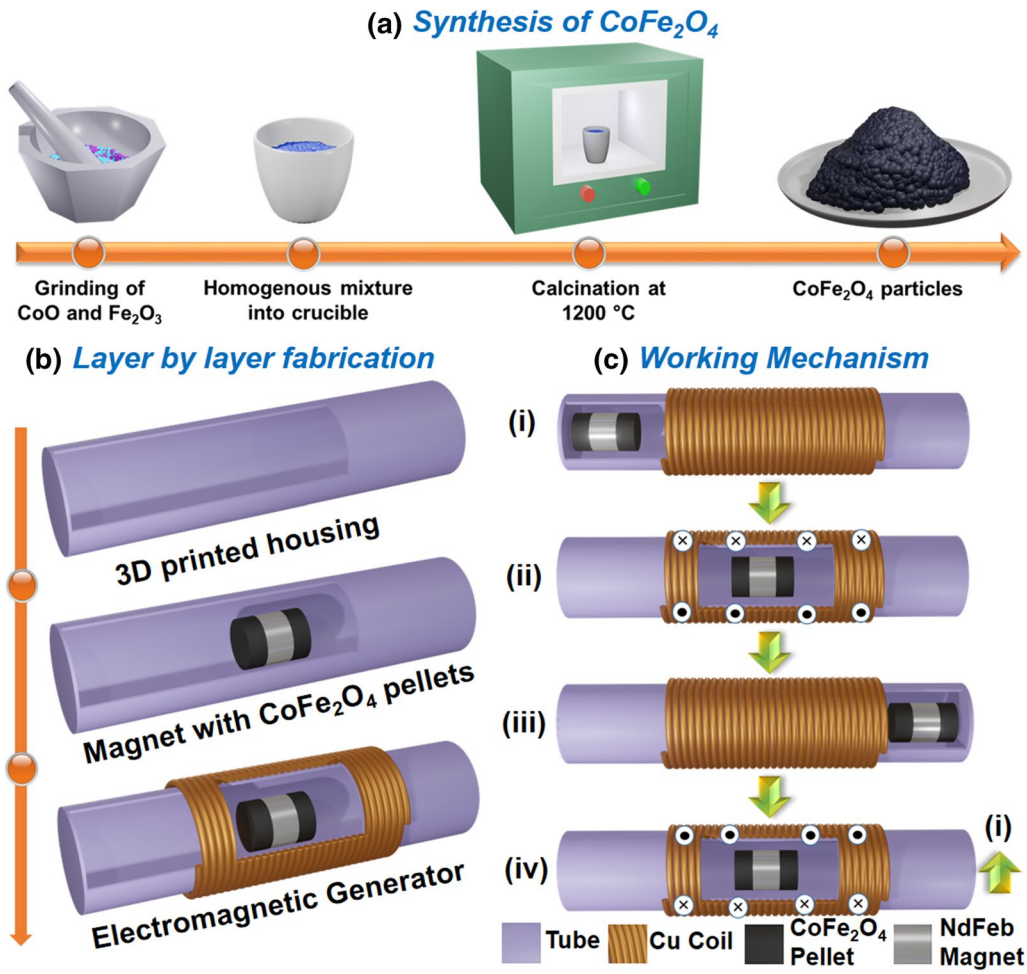

Fig. 1 (a) Synthesis of $CoFe_2O_4$ particles by solid-state reaction; (b) layer-by-layer fabrication technique to build the electromagnetic generator; (c) working mechanism of the electromagnetic generator.

with a dual nozzle and following a fused filament technology. The polylactic acid (PLA) was utilized to print the tube-like structure having a length of 80 mm and diameter of 20 mm.

Further, the arrangement of $CoFe_2O_4$ pellet/NdFeB magnet/$CoFe_2O_4$ pellet acted as the active magnetic component inside the tube. Copper wire having a diameter of 0.5 mm was wrapped across the tube with a maximum of 250 turns for fabrication of the EMG. The NdFeB magnet helped polarize the synthesized pellet. This type of arrangement could lead to the generation of electrical output from a resonating EMG. Figure 1c shows the working mechanism of the EMG: when the magnetic material or magnet is aligned with the coils, a magnetic flux ϕ and the output voltage of the EMG (V_{out}) can be written as

$$\Phi = BS \sin(n\omega t) \tag{1}$$

and

$$V_{out} = N = Nn\omega BS \cos(n\omega t), \tag{2}$$

respectively, where n represents pairs of magnets, N is the number of turns of coils, B is the magnetic induction, and S is the effective area of the coils. Figure 1c (i–iv) shows the steps of the generation of electrical output from an EMG. When the EMG device is shaken by hand, the magnet and magnetic material move across the coil inside the tube, generating the magnetic flux around the coil that induces the electron flow in the copper coil. As per Lenz's law, the electrical charge flow is influenced by the mobility of electrons. The electrical voltage and current response of the EMG device can be estimated following Faraday's law.

Figure 2a presents the room-temperature powder XRD patterns of the $CoFe_2O_4$ particles. The observed Bragg reflections at $2\theta = 30.16°$, 35.52°, 43.14°, 53.57°, 57.08°, 62.67°, and 74.12° correspond to (220), (311), (400), (422), (511), (440), and (533) plane characteristics of a single-phase and crystalline cubic $CoFe_2O_4$ ($Fd\bar{3}m$ (227) space

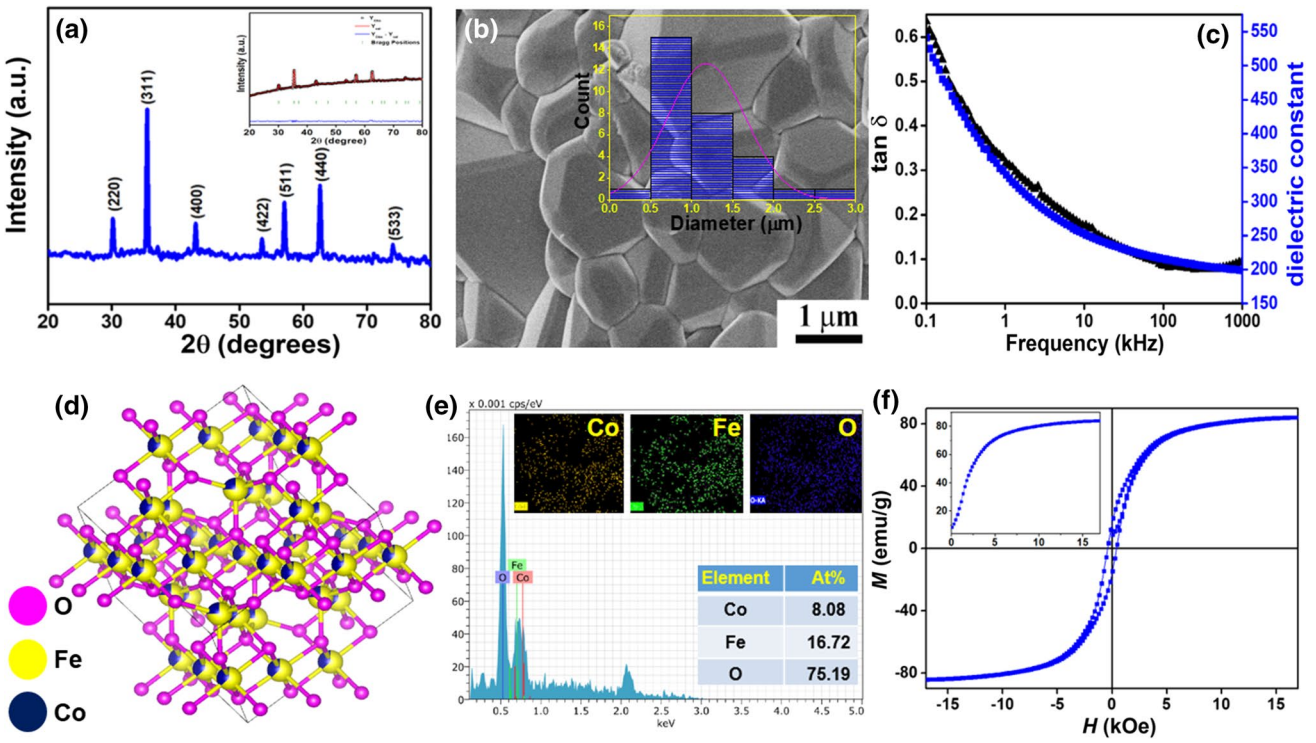

Fig. 2 (a) XRD analysis and (inset) Rietveld refinement; (b) surface micrograph; (c) dielectric constant and loss; (d) molecular structure; (e) EDS spectra with elemental mapping; and (f) room-temperature magnetic hysteresis (M-H) loop of the $CoFe_2O_4$ particles.

group, JCPDS no: 22-1086) spinel structure.[21] The absence of additional phases in the diffraction pattern within the experimental resolution ensures the phase purity of the sample. The average crystallite size (D) was determined by the classical Debye–Scherer equation,[22]

$$D = k\lambda/\beta \mathrm{Cos}\theta \tag{3}$$

where D is the average crystallite size, k is a constant value of 0.9 taken by assuming spherical particles, λ (= 1.54056 Å) is the wavelength of the x-ray, β is the full width at half maximum (FWHM) of the Bragg reflections (in radians), and θ is the diffraction angle of the corresponding Bragg reflections. The crystallite size was calculated to be ~30 nm from the highest intensity (311) reflection of the XRD pattern. Further, the Rietveld analysis given in the inset of Fig. 2a also confirms the inverse spinel structure, cubic symmetry, and lattice parameters of a = b = c = 8.391 Å. Figure 2b displays the polycrystalline nature of the $CoFe_2O_4$ sample with distinct grains and grain boundaries. No visible cracks and voids are observed. The average grain size of 1.18 μm is depicted from the histogram given in the inset. Figure 2c shows the dielectric constant and dielectric loss of the $CoFe_2O_4$ sample at room temperature over a wide range of frequencies. The dielectric constant and loss have higher values at lower frequencies, but the value decreases at high frequencies.[23] In the lower frequencies, the higher value of the dielectric constant arises from the different types of polarization active in that region, such as electronic, ionic, dipolar, or orientational, and space charge. At higher frequencies, dipoles could not follow the fast variation of the electrical field, leading to a decrease in dielectric constant and loss.[24] A dielectric constant of 510 was observed at 0.1 kHz. The molecular structure of the $CoFe_2O_4$ sample shown in Fig. 2d was designed from the crystallographic open database and crystallographic parameters. The EDS spectra show that all the elements are present in the natural surface of the sample, and the at% of the elements are presented in Fig. 2e. The elemental mapping clearly shows that there is no presence of impurity.

To confirm the magnetic behavior of our sample, the room-temperature magnetic hysteresis (M-H) measurement was carried out for the bulk $CoFe_2O_4$ sample, as presented in Fig. 2f. The inset of Fig. 2f shows the initial magnetization curve up to a maximum field of 17 kOe. The various magnetic parameters such as saturation magnetization (M_S), remanence magnetization (M_R), coercivity (H_C), and squareness ratio (M_R/M_S) were obtained from the M-H loop. The maximum magnetization (M_S) value is about 84.2 emu/g, which is in close agreement with the reported values of bulk $CoFe_2O_4$.[25–27] Further, the value of M_R was extracted from the M-H loop at the intersections of the loop with

the vertical magnetization axis and was ~ 16 emu/g. The squareness ratio (M_R/M_S) was found to be 0.19. Similarly, an H_C value of 409 Oe was obtained for the $CoFe_2O_4$ particles. It was previously reported that samples with large grain sizes prepared using solid-state technique show large magnetization but low M_R and H_C, which depict a predominant multi-domain feature.[27] Hence, the synthesized $CoFe_2O_4$ sample implies a multi-domain nature. However, an in-depth magnetic study is further required to quantify the correlative structural and magnetic behavior of the synthesized $CoFe_2O_4$ sample.

The electrical output of the EMG device is shown in Fig. 3a–b. The voltage and current response of the EMG device was recorded while shaking the device by hand, and it shows a voltage of about 1.95 V and a current of 4.7 mA. The long-term stability of the device is shown in Fig. 3c, where the device was subjected to handshaking motions, and the current output remained almost constant for 1500 s. It confirms that the EMG could easily convert the low-frequency motion into electrical energy. Figure 3d shows the load-matching analysis of the fabricated EMG device. The power of the device was calculated across various load resistance values. The formula used to calculate the power of the EMG at various load resistance was expressed as $P = V^2/R$ (P = power; V = voltage; and R = resistance). The highest power of 0.86 mW was achieved at a load resistance of 10^3 Ω. Further, in Fig. 3e, the charging of the 1-μF and 4.7-μF capacitor was carried out using a bridge rectifier and the EMG device. The bridge rectification circuit helps to convert the AC to DC output. The powering of LEDs in ON and OFF conditions is shown utilizing digital pictures in Fig. 3f.

Speed sensors are widely used in industrial testing systems to gain insight into construction or drilling tools. These sensors commonly use a battery to operate and generally follow a centrifugal, capacitive, or magnetic mechanism. Hence, it is necessary to find an alternative by developing self-powered sensors to monitor the vibration and operation speed. Figure 4a shows the digital image of the fabricated EMG and EMG device connected on a shaker. Figure 4b–c shows the voltage response of the EMG device when the shaker is operated at different speeds. This type of self-powered recognition of the vibration or speed of machines can be useful to understand and monitor the damage or healthy state of a machine.

Conclusion

In conclusion, single-phase high-purity $CoFe_2O_4$ was synthesized by a high-temperature solid-state reaction. The XRD data reveal a cubic symmetry, and EDS spectra confirm the elemental compositions. The magnetic property of the $CoFe_2O_4$ reveals a high saturation magnetization value of 84.2 emu/g. Further, the device applications of these synthesized particles were tested by fabricating an

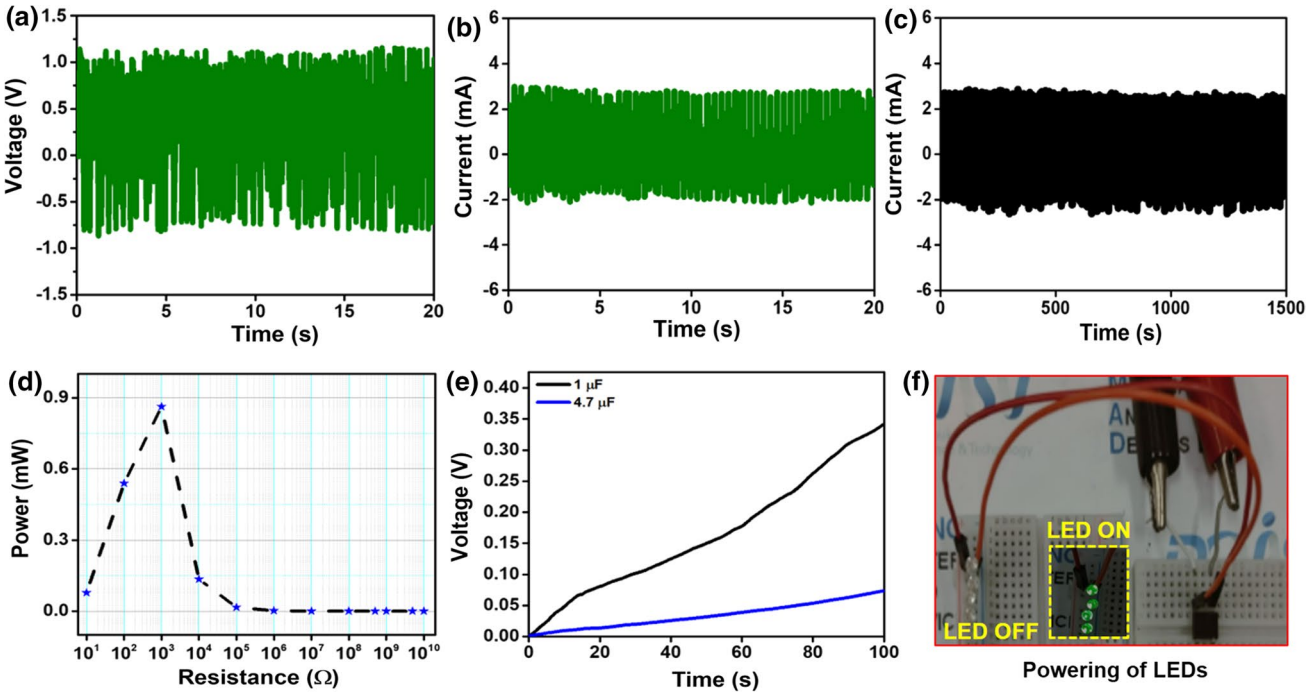

Fig. 3 (a) Voltage; (b) current response; (c) stability of response of the electromagnetic generator; (d) calculated power output at various load resistance values; (e) charging of various capacitors using the EMG; and (f) powering of LEDs.

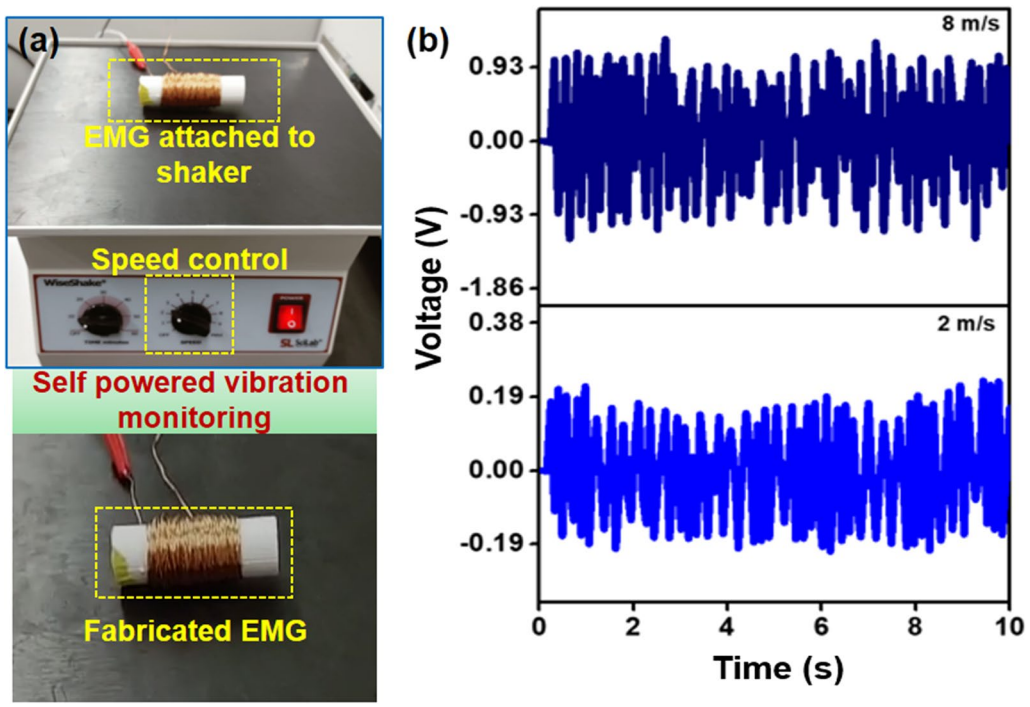

Fig. 4 (a) Digital image of the EMG attached to a vibrational shaker; (b, c) voltage response of the EMG devices at different speeds of shaking or vibrations.

electromagnetic generator. An electrical voltage of 1.95 V and current of 4.7 mA were generated while delivering a power output of 0.86 mW at a load resistance of 10^3 Ω. The demonstration of powering of LEDs and charging of capacitors confirms that this fabricated device can act as a sustainable power source. The self-powered recognition of shaker speed and vibration elucidates its usage in many other useful applications in daily life, such as earthquake monitoring, structural health monitoring, and machine fault detection.

Supplementary Information The online version contains supplementary material available at https://doi.org/10.1007/s11664-022-09551-5.

Acknowledgments This study is supported by Basic Science Research Program through the National Research Foundation of Korea (NRF), funded by the Ministry of Science and ICT of Korea (2021R1C1C1011588). The authors declare that they have no conflict of interest.

Authors' Contributions YO: Investigation, methodology. MS: Writing—original draft, data curation. SH: Writing—original draft, formal analysis. AMP: Formal analysis. SP: Data curation. HJK: Supervision, writing—review & editing, funding acquisition.

Conflict of interest The authors declare no conflict of interest.

References

1. R. Li, Y. Liao, Y. Dou, D. Wang, G. Li, W. Sun, J. Wu, and Z. Lan, *Sol. Energy* 220, 400 (2021).
2. K.L. Routray, S. Saha, and D. Behera, *Phys. Status Solidi B* 256, 1800676 (2019).
3. H. Wu, Q. Zhang, C. Wan, S.S. Ali, Z. Yuan, L. You, J. Wang, Y. Choi, and X. Han, *IEEE Trans. Magn.* 51, 1 (2015).
4. R. Zhang, L. Sun, Z. Wang, W. Hao, E. Cao, and Y. Zhang, *Mater. Res. Bull.* 98, 133 (2018).
5. M. Cernea, P. Galizia, I. Ciuchi, G. Aldica, V. Mihalache, L. Diamandescu, and C. Galassi, *J. Alloy. Compd.* 656, 854 (2016).
6. D. Jnaneshwara, D. Avadhani, B.D. Prasad, B. Nagabhushana, H. Nagabhushana, S. Sharma, C. Shivakumara, J. Rao, N. Gopal, and S.-C. Ke, *J. Magn. Magn. Mater.* 339, 40 (2013).
7. I. Nlebedim, N. Ranvah, P.I. Williams, Y. Melikhov, J.E. Snyder, A.J. Moses, and D. Jiles, *J. Magn. Magn. Mater.* 322, 1929 (2010).
8. L. Kumar, and M. Kar, *J. Magn. Magn. Mater.* 323, 2042 (2011).
9. A. Hossain, M. Sarker, M. Khan, and M. Rahman, *Mater. Sci. Eng. B* 253, 114496 (2020).
10. Z. Zi, Y. Sun, X. Zhu, Z. Yang, J. Dai, and W. Song, *J. Magn. Magn. Mater.* 321, 1251 (2009).
11. S.K. Karan, S. Maiti, J.H. Lee, Y.K. Mishra, B.B. Khatua, and J.K. Kim, *Adv. Func. Mater.* 30, 2004446 (2020).
12. M. Sahu, S. Hajra, H.-G. Kim, H.-G. Rubahn, Y. Kumar Mishra, and H.J. Kim, *Nano Energy* 88, 106255 (2021).

13. S. Hajra, M. Sahu, A.M. Padhan, I.S. Lee, D.K. Yi, P. Alagarsamy, S.S. Nanda, and H.J. Kim, *Adv. Func. Mater.* 31, 2101829 (2021).
14. T. Quan, Y. Wu, and Y. Yang, *Nano Res.* 8, 3272 (2015).
15. Y.S. Choi, S.-W. Kim, and S. Kar-Narayan, *Adv. Energy Mater.* 11, 2003802 (2021).
16. C.R. Saha, T. O'Donnell, H. Loder, S. Beeby, and J. Tudor, *IEEE Trans. Magn.* 42, 3509 (2006).
17. A. Ahmed, I. Hassan, A.S. Helal, V. Sencadas, A. Radhi, C.K. Jeong, and M.F. El-Kady, *iScience* 23, 101286 (2020).
18. G. Lin, H. Wang, X. Li, X. Lai, Y. Zou, X. Zhou, D. Liu, J. Wan, and H. Xin, *Sens. Actuators B Chem.* 255, 3364 (2018).
19. S. Divya, K. Jeyadheepan, and J. Hemalatha, *J. Magn. Magn. Mater.* 492, 165689 (2019).
20. B. Rani, and N.K. Sahu, *Diam. Relat. Mater.* 108, 107978 (2020).
21. V.H. Ojha, and K.M. Kant, *J. Phys. Chem. Solids* 148, 109655 (2021).
22. M. Basak, M.L. Rahman, M.F. Ahmed, B. Biswas, and N. Sharmin, *Mater. Chem. Phys.* 264, 124442 (2021).
23. P. Sharma, S. Hajra, S. Sahoo, P.K. Rout, and R.N.P. Choudhary, *Process. Appl. Ceram.* 11, 171 (2017).
24. K. Lee, S. Hajra, M. Sahu, and H.J. Kim, *J. Alloys Compd.* 882, 160634 (2021).
25. A. Das, K. Kumar Bestha, P. Bongurala, and V. Gorige, *Nanotechnology* 31, 335716 (2020).
26. A. Barik, M.R. Sahoo, S. Tiwary, R. Ghosh, and P.N. Vishwakarma, *AIP Conf. Proc.* 2265, 030533 (2020).
27. P.R. Varma, R.S. Manna, D. Banerjee, M.R. Varma, K. Suresh, and A. Nigam, *J. Alloy. Compd.* 453, 298 (2008).